

Article

Utilization of Loaded Cobalt onto MCM-48 Mesoporous Catalyst as a Heterogeneous Reaction in a Fixed Bed Membrane Reactor to Produce Isomerization Product from *n*-Heptane

Nisreen S. Ali ¹, Issam K. Salih ², Hamed N. Harharah ³ , Hasan Sh. Majdi ² , Hussein G. Salih ⁴,
Khairi R. Kalash ⁵ , Ali Al-Shathr ⁴ , Farah T. Al-Sudani ⁴, Mahir A. Abdulrahman ⁴ , Jamal M. Alrubaye ⁴,
Talib M. Albayati ^{4,*} , Noori M. Saady ⁶  and Sohrab Zendejboudi ⁷ 

- ¹ Materials Engineering Department, College of Engineering, Mustansiriyah University, Baghdad P.O. Box 14022, Iraq; nisreensabah@uomustansiriya.edu.iq
- ² Department of Chemical Engineering and Petroleum Industries, Al-Mustaqbal University, Babylon 51001, Iraq; dr_issamkamil@mustaqbal-college.edu.iq (I.K.S.); hasanshker1@gmail.com (H.S.M.)
- ³ Department of Chemical Engineering, College of Engineering, King Khalid University, Abha 61411, Saudi Arabia; hhharharah@kku.edu.sa
- ⁴ Department of Chemical Engineering, University of Technology—Iraq, 52 Alsinaa St., Baghdad P.O. Box 35010, Iraq
- ⁵ Environment and Water Directorate, Ministry of Science and Technology, Baghdad 10070, Iraq
- ⁶ Department of Civil Engineering, Memorial University, St. John's, NL A1B 3X5, Canada
- ⁷ Department of Process Engineering, Memorial University, St. John's, NL A1B 3X5, Canada
- * Correspondence: talib.m.naieff@uotechnology.edu.iq



Citation: Ali, N.S.; Salih, I.K.; Harharah, H.N.; Majdi, H.S.; Salih, H.G.; Kalash, K.R.; Al-Shathr, A.; Al-Sudani, F.T.; Abdulrahman, M.A.; Alrubaye, J.M.; et al. Utilization of Loaded Cobalt onto MCM-48 Mesoporous Catalyst as a Heterogeneous Reaction in a Fixed Bed Membrane Reactor to Produce Isomerization Product from *n*-Heptane. *Catalysts* **2023**, *13*, 1138. <https://doi.org/10.3390/catal13071138>

Academic Editors: José Antonio Calles and Anastasia Macario

Received: 22 June 2023

Revised: 12 July 2023

Accepted: 17 July 2023

Published: 22 July 2023



Copyright: © 2023 by the authors. Licensee MDPI, Basel, Switzerland. This article is an open access article distributed under the terms and conditions of the Creative Commons Attribution (CC BY) license (<https://creativecommons.org/licenses/by/4.0/>).

Abstract: The use of catalytic membranes as microstructured reactors without a separative function has proved effective. High catalytic activity is possible with minimal mass transport resistances if the reactant mixture is pushed to flow through the pores of a membrane that has been impregnated with catalyst. In this study, *n*-heptane (C₇H₁₆) was hydrocracked and hydro-isomerized within a plug-flow zeolitic catalytic membrane-packed bed reactor. The metallic cobalt (Co) precursor at 3 wt.% was loaded onto support mesoporous materials MCM-48 to synthesize heterogeneous catalysis. The prepared MCM-48 was characterized by utilizing characterization techniques such as scanning electron microscopy (SEM), X-ray diffraction (XRD), energy dispersive X-ray analysis (EDAX), Fourier transform infrared (FTIR), nitrogen adsorption–desorption isotherms, and the Brunauer–Emmett–Teller (BET) surface area. The structural and textural characteristics of MCM-48 after encapsulation with Co were also investigated. The analyses were performed before and after metal loading. According to the results, the 3 wt.% Co/MCM-48 of metallic catalyst in a fixed bed membrane reactor (MR) appears to have an excellent catalytic activity of ~83% during converting C₇H₁₆ at 400 °C, whereas a maximum selectivity was approximately ~65% at 325 °C. According to our findings, the synthesized catalyst exhibits an acceptable selectivity to isomers with multiple branches, while making low aromatic components. In addition, a good catalytic stability was noticed for this catalyst over the reaction. Use of 3 wt.% Co/MCM-48 catalyst led to the highest isomerization selectivity as well as *n*-heptane conversion. Therefore, the heterogeneous catalysis MCM-48 is a promising option/ alternative for traditional hydrocracking and hydro-isomerization processes.

Keywords: catalytic reactor; catalyst characterization; selectivity; metallic catalyst; reaction kinetics; isomerization

1. Introduction

Integrating membrane separation and reaction system in a single process unit exhibits considerable advantages compared to conventional process systems [1]. This promising concept has been introduced for a variety of applications in chemical and process engineering where chemical and biochemical reactors and membranes are involved [2]. This

integration strategy is labeled with three common categories, including contactor, distributor, and extractor. In general, membranes are called flow-through catalytic membrane reaction systems [3]. Hydro-isomerization of paraffins is an interesting process to enhance the gasoline octane number via replacing the normal paraffin by branched paraffin [4,5]. Otherwise, straight naphtha often undergoes isomerization or hydro-isomerization catalytic reaction to increase the octane number and upgrade the quality of products [6–8]. Thermodynamically, this catalytic process is desired at low temperatures using an acid catalyst; however, it requires an especial catalyst type such as bifunctional catalyst at high temperatures ~ 500 °C [9–15]. This high temperature condition leads towards cracking reaction which acts to reduce the production of desired products [5,16–18]. Therefore, the aim of hydro-isomerization process should be to maximize gasoline octane at low temperature active catalysts with recycling flow techniques for isomers that have low octane number. The selectivity of isomers is the main criterion that should be measured to evaluate the catalyst suitability. One of the promising microporous materials utilized in different catalytic reactions are zeolites with porous crystalline structures made of aluminosilicate materials; they are generally employed as catalysts and adsorbents in chemical and energy industries. For instance, petrochemical processes such as hydrocracking and catalytic cracking widely utilize synthetic zeolites with mesoporous structures (e.g., MCM-41) as the catalysts. Zeolite membrane sieves are widely used as an alternative to fractionation for recycled normal paraffins owing to it being more energy efficient and having a selective separation technique [19–24]. It is defined as a substance that is used to separate gas or liquid mixture by accelerating the reaction through diminishing the activation energy. The interest in zeolite membranes has increased since the beginning of the present century due to it being employed as a catalyst in several reactions such as hydro-isomerization, isomerization, esterification, alkylation, and dehydrogenation [25,26]. Although the zeolite membrane is fragile and crisp, it is considered to be a thermally stable and to have very good chemical resistance compared with the pure polymer membrane. Several research works about the potential of zeolite layers for the synthesis of innovative as well as complex active materials, such as dielectrics with mechanical stability, molecular sensors, and advanced reaction-diffusion systems, have recently discussed. In the era of nanotechnology, layers of organised porous molecular sieve are considered to be extremely useful materials with cutting-edge applications [27,28]. Simply, combining a zeolite catalyst with a membrane becomes necessary during the separation of linear molecules from the product mixture by the membrane, and then they are fed directly over the zeolite catalyst to form mono- and di-branched molecules [29,30]. Gora and Jansen [31] employed a membrane reactor to study the hydro-isomerization of *n*-heptane over a combination of platinum chlorinated alumina as a catalyst with silicalite-1 zeolite as a membrane. They concluded that the combination of zeolite membrane with a Pt-loaded chlorinated catalyst contributed to improving the octane number. The interest in mesoporous compound MCM-48 increased after 1992 when Mobil Oil researchers discovered it [32,33]. It has attracted the attention of numerous researchers owing to its prospective uses as a catalyst, adsorbent, and catalyst support. The main features of MCM-48 are that it has high thermal stability, large surface areas around $1000\text{--}1500$ m² g⁻¹, specific pore volume reaching up to ~ 1.2 cm³ g⁻¹, and narrow distribution of pore sizes of 1.45–1.72 nm [34–39].

In this paper, the synthesis, characterization, and application of MCM-48 in a membrane reactor through hydro-isomerization and a hydrocracking reaction process are presented. In contrast to previous membrane reactor designs, no separation work is carried out. Catalytically active porous membranes, which are often made of an amorphous silica wall, are used since perm selectivity is not necessary. The membrane's role is to enable the close proximity of the reactants and catalyst, brief contact times, and a restricted distribution of residence times. Few studies were of interest about the loaded cobalt onto the MCM-48 nanoporous catalyst employed in the *n*-heptane hydro-isomerization. Therefore, in the present study, the catalytic activity of MCM-48-supported at 3 wt.% of Co

catalysts, which serves as an MR for reactions involving *n*-heptane in hydro-isomerization and hydrocracking, was investigated.

2. Results and Discussion

2.1. Characterization

The XRD patterns with small angles of samples of the MCM-48 membrane calcined for 4 h at 500 °C are presented in Figure 1. These patterns revealed a mesostructure indicating peak of intense diffraction (1 0 0) at around 2θ of 2.56° for 3 wt.% Co/MCM-48 and 2.53° for MCM-48. Furthermore, two further peaks, categorized as (2 1 1) and (2 2 0), were observed in the XRD patterns. A sequence of small peaks situated between 3.5 and 5.5° and two reflection peaks at 2θ lower values than 3° are matched to the cubic structure of Ia₃d. The peaks observed in this research strongly resemble the corresponding peaks described in the literature [40–42].

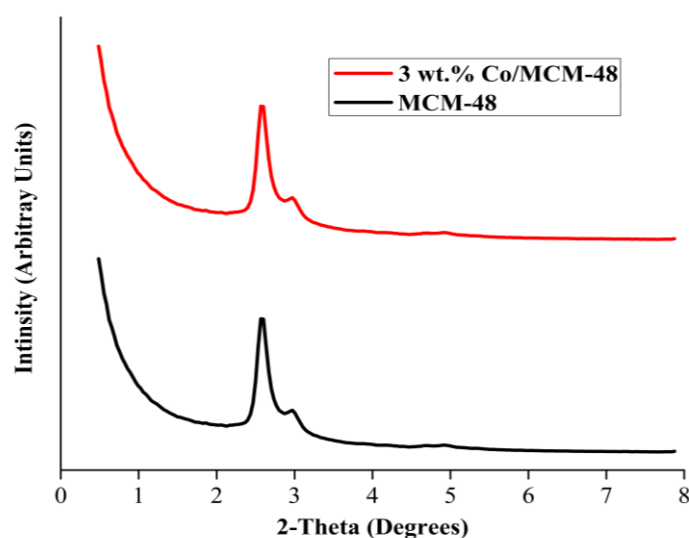


Figure 1. X-ray diffraction pattern of MCM-48 and 3 wt.% Co/MCM-48.

The N₂ adsorption–desorption isotherms for the siliceous MCM-48 and 3 wt.% Co/MCM-48 catalysts are depicted in Figure 2. The curves of the samples follow the usual cubic MCM-48 mesoporous material Langmuir IV adsorption isotherms, which are complemented by an H1-type hysteresis loop. The textural characteristics of the composite materials are shown in Table 1 for comparison purpose. The results indicate that composite catalysts and MCM-48 have excellent S_{BET} . The pore volume (V_{P}) for the prepared 3 wt.% Co/MCM-48 catalyst is less than V_{P} for MCM-48. The type IV isotherm and the type H1 hysteresis loop are related to isotherms of nitrogen adsorption of MCM-48 (see Figure 2); the sharp branches of adsorption and desorption in hysteresis loops are evidence of a narrow distribution of pore sizes. Generally, the height and sharp appearance of the capillary condensation stage in the isotherms demonstrate the uniformity of the pore size for mesoporous molecular sieves [43]. Figure 2 displays the typical type IV isotherm for the MCM-48, with a common capillary condensation scene leading to symmetrical mesoporous in the 0.05 to 0.25 relative pressure (P/P_0) range. Table 1 lists the structural parameters derived from measurements of nitrogen adsorption, which display the specific surface area, wall thickness, pore size, and pore volume of the sample.

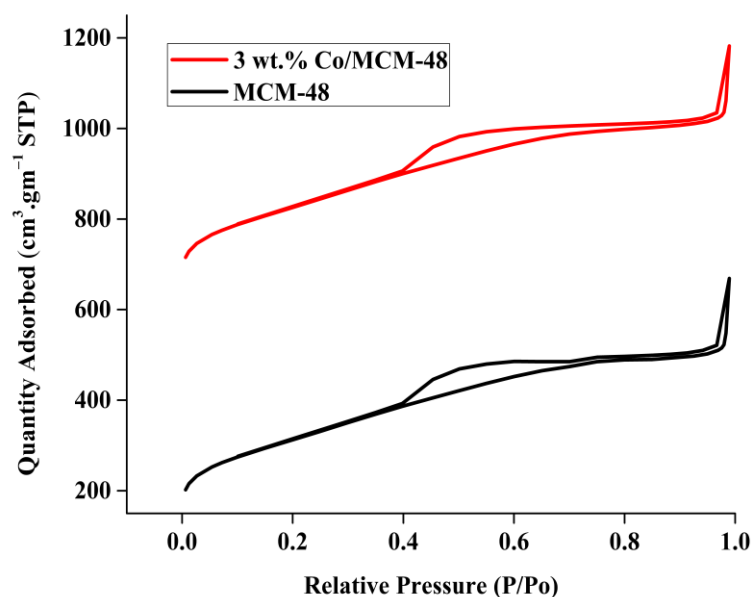


Figure 2. Nitrogen adsorption-desorption isotherms for MCM-48 and 3% Co/MCM-48.

Table 1. BET surface area, pore volume, and pore size of MCM-48.

Sample	S_{BET} ($\text{m}^2 \cdot \text{g}^{-1}$)	V_{P} ($\text{cm}^3 \cdot \text{g}^{-1}$)	$V_{\mu\text{P}}$ ($\text{cm}^3 \cdot \text{g}^{-1}$)	D_{P} (nm)	α_0 (nm)	t_{wall} (nm)
MCM-48	1400	1.3	0.4	3	4	0.5
3 wt.% Co/MCM-48	800	0.8	0.05	4	3	0.3

Figure 3 shows the pore size distribution (PSD) of the 3 wt.% Co/MCM-48 catalytic membrane and MCM-48. The wide size distributions of pores for the substance manufactured utilizing CTAB, NaOH, and TEOS were centered at 34 Å. For the basic preparation, a considerable number of mesopores were observed, providing the most obvious distribution of pore sizes and demonstrating a remarkably usual structure [35,38].

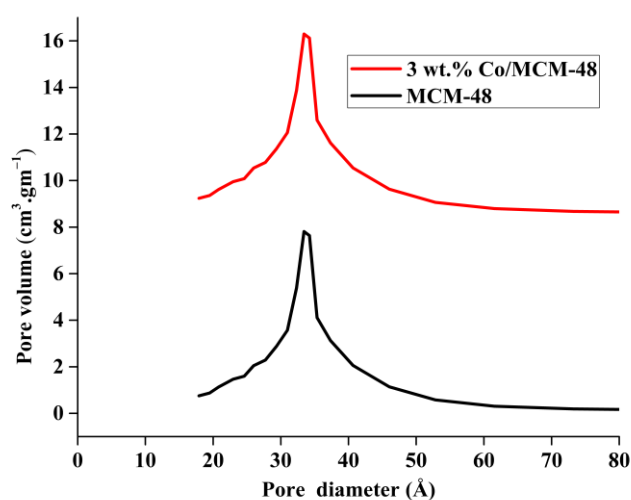


Figure 3. BJH pore size distribution of MCM-48 and 3 wt.% Co/MCM-48.

The MCM-48 and composites' FT-IR spectra indicate a vibration band about 3400 cm^{-1} , which is attributed to OH (H_2O). The FT-IR spectra of MCM-48 are shown in Figure 4, and it exhibits the standard Si-O-Si bands at bands of 1080 , 960 , 800 , and 459 cm^{-1} , which are the result of the stretching vibration in Si-O-Si. The 960 cm^{-1} absorption band can be attributed

to either Si-O-Si or Si-OH vibration of stretching. The large band at about 3463 cm^{-1} is due to the existence of exterior OH groups and the intense hydrogen-bonding connections between them by the Si-OH groups. Eventually, it is feasible to identify the band at roughly 1637 cm^{-1} as the base of the distortion behaviour of OH bonds of adsorbed H_2O [44,45]. The spectrum characteristics of a loaded metal Co are quite identical to MCM-48 owing to its low metal content, while the samples' two further bands are the black arrows that appear at 660 and 570 cm^{-1} . Metals have slightly stronger Co/MCM-48 bands than MCM-48. The adsorption bands of 3454 cm^{-1} and 1631 cm^{-1} (to bending vibration of O-H) are attributed to stretching vibration and water moisture, respectively, based on the FT-IR spectrum of Co. The peak at 690 cm^{-1} was considered as the characteristic peak of Co. [46]. We relate this to the existence of bigger particles size on the exterior side of the catalyst pores, since Co/MCM-48 reveals similar absorbance bands in a way that dramatically increases in intensity [42].

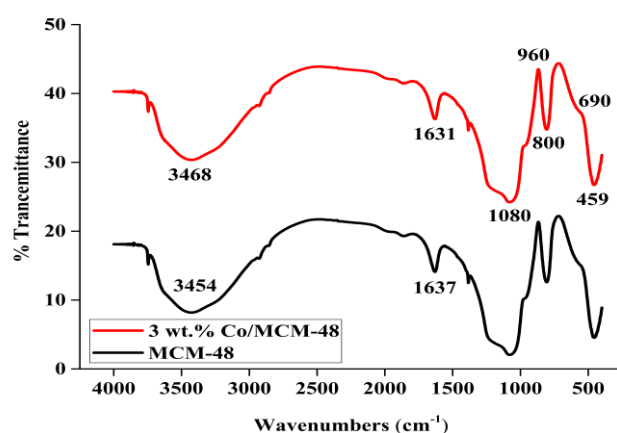


Figure 4. FT-IR spectra of MCM-48 and 3% Co/MCM-48.

The systematic MCM-48 and 3 wt.% Co/MCM-48 were exposed to EDAX and SEM characterization tests. Figure 5 (panels a and c) clearly demonstrate SEM images of both of these materials at a $1000\times$ magnification. Scanning electron microscopy (SEM) pictures of the MCM-48 and 3 wt.% Co/MCM48 are depicted in Figures 5a and 5c, respectively. The SEM picture of the siliceous MCM-48 had a spherical shape and was similar in particle size, as can be seen in Figure 5. Note that the particle size of composite catalysts is not constant, as evident from Figure 5.

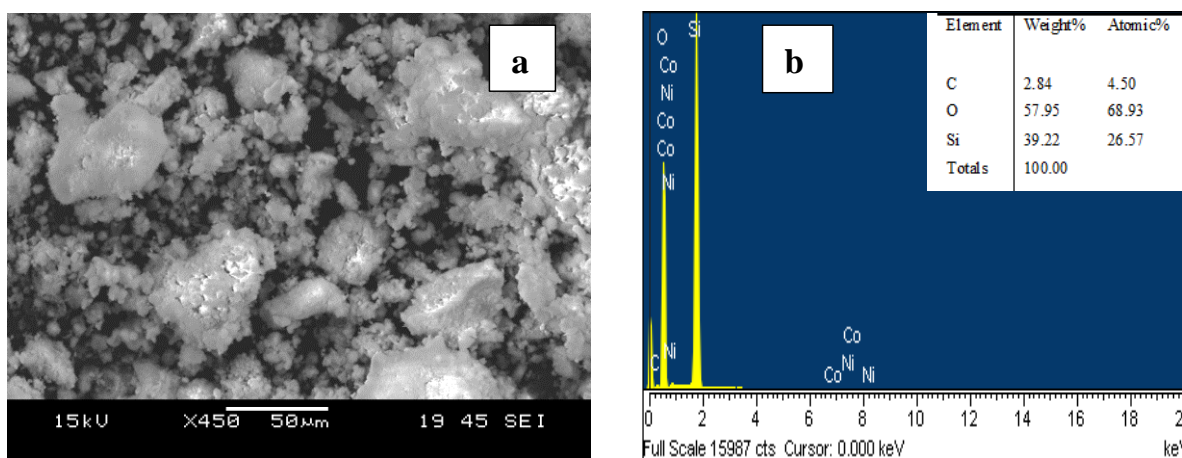


Figure 5. Cont.

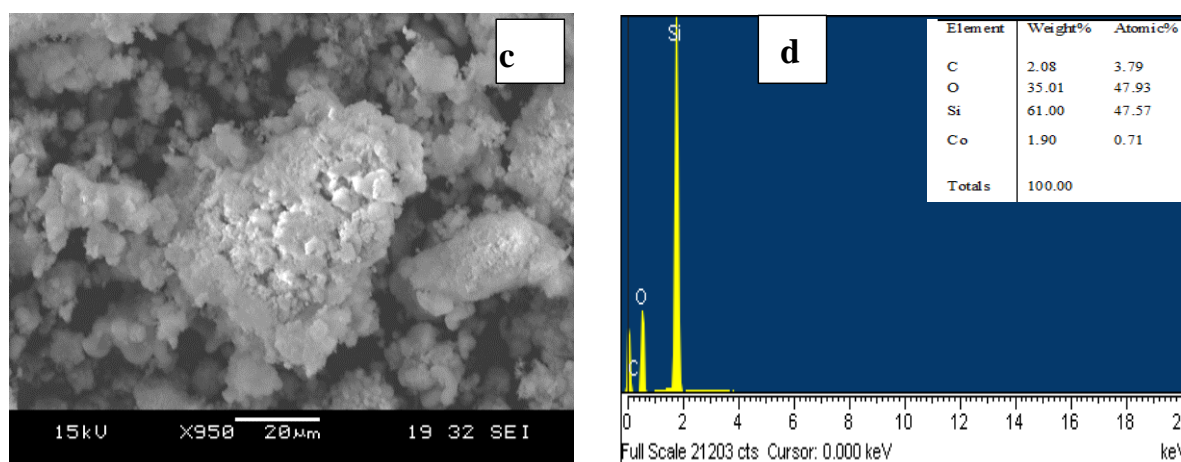


Figure 5. (a) SEM image of MCM-48, (b) EDX image for pure MCM-48, (c) SEM image of 3% Co/MCM-48, and (d) EDAX image for 3% Co/MCM-48.

Pre-test catalyst samples were exposed to EDAX. Panels b and d of Figure 5 include EDAX figures for MCM-48 and 3%Co/MCM-48, respectively. The MCM-48 nanoporous material produced peaks on the EDAX graph that indicated the zeolite was generally formed by the combination of C, O, and Si, whereas the metals loaded are represented by the peaks in Figure 5d. EDAX graphs were made for a variety of different positions on the SEM images to obtain a precise average weight percentage for every material [44]. The ratio of Si/O over the MCM-48 tested samples can be approximately estimated from the weight percentages of Si and O predicted by these figures. It was observed that the Si/O ratios for MCM-48 and 3% Co/MCM-48 are around 0.68 and 1.7, respectively.

2.2. Conversion of *n*-Heptane

Measurements of the experimental data were made with a Co-loaded MCM-48. In Figure 6, the isomerization of *n*-C₇ over this catalyst between 200 and 400 °C served as a measure of the catalyst activity. As can be observed from the conversion findings, increasing the reaction temperature to 400 °C enhanced the *n*-C₇ conversion practically linearly. For the Co/MCM48 catalyst, the maximum conversion was observed. Catalytic activity was shown to depend on a number of variables, including surface qualities, metal function, structural regularity, distribution, kind of acid sites, geometry, and strength. The following equation was used to determine the overall conversion for the catalytic membrane at 3 wt.% Co/MCM-48 in weight percentage under various temperature conditions while preserving a steady flow rate of 20 mL min⁻¹.

$$\% \text{ Conversion of } n - \text{heptane} = 100 \left[\frac{\text{no. of moles of } n - \text{heptane consumed}}{\text{no. of moles of } n - \text{heptane introduced}} \right] \quad (1)$$

The calculated conversion for the catalytic membrane with 3 wt.% Co investigated at various temperature ranges with a constant *n*-C₇ flow rate of 0.287 mL/min is shown in Figure 6. The activity of the MCM-48 catalytic membrane is due to the existence of Lewis acid sites in the catalyst structure. With a conversion rate reaching 83% at 400 °C, the catalytic membrane composed of 3 wt.% Co/MCM-48 exhibits the next-best conversion when temperatures are at the highest level. It may be observed that tri-metallic 3 wt.% Co/MCM-48 has greater membrane reactor activity because of the size of the metal cluster [47,48].

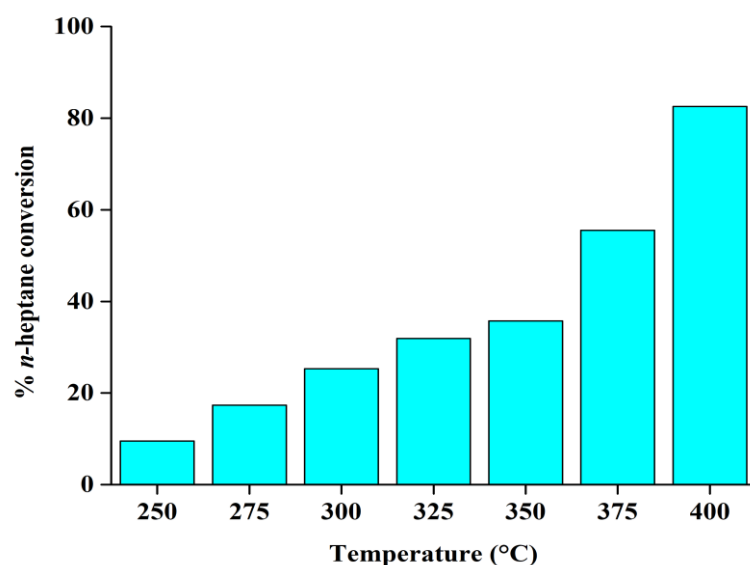


Figure 6. Conversion of *n*-heptane for the tested catalytic membrane.

2.3. Selectivity to Isomerization

For a catalytic membrane including 3 wt.% Co/MCM-48, estimations were conducted to evaluate the selectivity of isomerization products (*i*-C₇) by using the below equation as shown in Figure 7.

$$\% \text{ Selectivity to } i\text{-heptane} = 100 \times \left[\frac{\sum i\text{-heptane (g)}}{\sum \text{Total Products (g)}} \right] \quad (2)$$

Figure 7 demonstrates the selectivity of isomerization products at various operating temperatures within the MR that includes the 3 wt.% Co/MCM-48 catalytic membrane. The intermediate alkenes can be transformed into their structural isomers as a result of the Lewis acid sites' abundance of zeolite throughout the mechanism of the isomerization reaction across tri-functional catalysts. When these acid sites are missing, such as in the situation on MCM-48, only processes involving hydrocracking and dehydrogenation are possible [49,50].

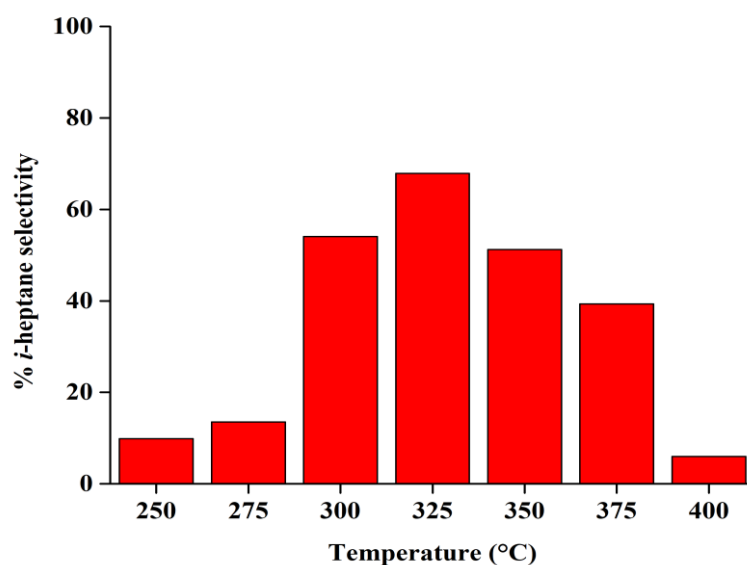


Figure 7. Isomerization product selectivity for the tested catalytic membrane.

Since the catalytic membrane of MCM-48 has larger pores, it has poor isomerization product selectivity and is hence non-product selective. For instance, MCM-48 exhibits a 3.5 nm pore diameter, while cyclohexane has a 0.6 nm molecular diameter, which measures six times smaller. As a result, the molecules of the reactant react and leave the pores of the catalyst prior to the development of any selectivity [50]. Chica and Corma (1999) investigated production of gasoline with high octane number through hydroisomerization of *n*-heptane to dibranched and tribranched components where different zeolites such as unidirectional 12 Membered Ring (MR) zeolites having various pore sizes were employed [51].

2.4. Selectivity to Cracking

According to the results of this study, all the catalyst cases have high selectivity isoheptane (i-C7) at low reaction temperature and/or low conversion, due to thermodynamic constraint of the isomerization reaction. It has been proven that the isomer formation, desorption, and diffusive mass transfer in the tiny catalyst pores experience delay in most catalyst samples, since the multi-branched isomers have higher molecular size compared to the mono-branched ones. This usually leads to production of more cracking components. Referring to our results, the introduced catalysts show promising selectivity to isomers with multiple branches. It was found that the catalyst pore diameter has a vital role in synthesis of the multi-branched C7. The selectivity of cracking, hydrogenolysis products, and aromatization of *n*-C7 in terms of reaction temperature are demonstrated in Figure 8. Based on the literature, the existence of mesoporosity expedites hydrogen transfer reactions between cyclic intermediates and olefin. Thus, cracking and aromatization are considered as the key reactions of all mesoporous cases. Note that the reactions cause an increase in the magnitude of yields of LPG and aromatics. Furthermore, increasing temperature can increase the amount of cracking and aromatic products. The balance between acid and metal functions, geometry, acidity, and type of acid location mainly influence the reactions and their extents. Based on our results, the introduced catalyst exhibits a good selectivity with respect to desired products (e.g., aromatization and isomerization products). As it is clear from Figure 8, a very low amount of aromatics is produced upon utilization of the composite catalyst. It is worth noting that aromatic parts have an elevated level of octane number in gasoline. However, synthesis of reformulated gasoline with low benzene concentration is an important strategy in the petrochemical industry, due to environmental regulations. The isomerization of *n*-paraffin is a key reaction to enhance octane number. For all of the temperatures that were measured, with an *n*-C7 flow rate of 0.28 mL per minute, the selectivity for cracked products (C₁–C₆) by the 3 wt.% Co/MCM-48 catalytic membrane was determined by the following equation:

$$\% \text{ Selectivity to Cracking} = 100 \times \left[\frac{\sum \text{Cracked Product (g)}}{\sum \text{Total Products (g)}} \right] \quad (3)$$

Figure 8 demonstrates the results of the temperature tests used to assess the membrane cracking selectivity of 3 wt.% Co/MCM-48. It shows clearly that the selectivity to cracking rises to 98 wt.% at 400 °C. Again, owing to the structure of the catalyst pore and the abundance of Lewis acid sites, the catalytic membrane of the MCM-48 reveals a higher selectivity for cracked products. Alongside being active, the MCM-48 catalytic membrane is structurally non-selective for the hydro-isomerization of *n*-C₇ such as the targeted isomerization products and insufficient Bronsted acid sites that contribute to isomerization. As confirmed in the literature [30], hydro-isomerization processes and hydrocracking reactions are in thermodynamic equilibrium and usually occur between 210 and 270 °C, which is a relatively low temperature. Since hydro-isomerization requires low temperatures, the catalytic membrane of MCM-48 is inactive and exhibits no selectivity for isomerization products at these temperatures. Thus, the MCM-48 catalytic membrane demonstrates a significant selectivity towards cracked products regarding the operation at a relatively high temperature between 300 and 400 °C as a consequence of the structure of the catalyst, which contains Lewis acid sites. The same conclusion was obtained by Tan et al. [52,53].

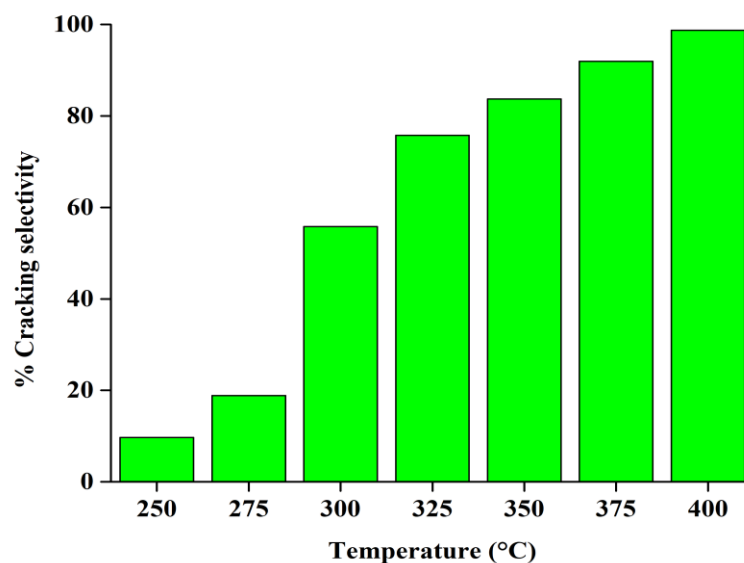


Figure 8. Cracking product selectivity for the tested catalytic membrane.

It follows that the selectivity of the catalyst for iso-heptane (*i*-C7) is high at low conversion or low reaction temperatures as a result of the thermodynamic limit of the isomerization process. According to the literature, isomer production is frequently challenging. As a result of the multi-branched isomers' larger molecular size compared to mono-branched isomers, their synthesis, desorption, and diffusion inside the narrow pores would be impeded in most catalysts, which typically leads to more cracking products. However, our study shows that the introduced catalyst has a strong affinity for multi-branched isomers. This finding suggests that our catalysts' pore diameters are important in the production of multi-branched C7. The selectivity of the *n*-C7's hydrogenolysis, aromatization, and cracking products versus reaction temperatures is shown in Figure 8. Various examples in the literature demonstrate that the presence of mesoporosity promotes the hydrogen transfer processes between cyclic intermediates and olefins. The primary responses of all mesoporous materials are hence aromatization and cracking. Increased yields of aromatics and LPG are produced as a result of these reactions. The rate of cracking and the production of aromatic compounds also rise as the temperature goes up [52]. The literature reveals that the bi-functional nature catalyst is made of highly amorphous silica, resulting in the catalyst acidic characteristic/nature. The MCM-48 cubic matrix is coated with 3 wt.% cobalt. It should be noted that cobalt in the presence hydrogen could result in coke deposition prevention; this will then improve the catalyst activity.

Acidity, acid type, acid position, geometry, and the balance between the functions of the acid and the metal all play a role in this reaction's competition with other reactions. Based on the study outputs, our synthetic catalyst has a good selectivity for desired products such isomerization and aromatization products. With this composite catalyst, very little aromatic molecule synthesis occurs, as seen in Figure 8. The octane rating of gasoline for aromatic compounds is high. The petrochemical industry's primary goal, however, is to produce reformulated gasoline with reduced benzene levels owing to environmental laws. One advantageous process for raising octane is the isomerization of *n*-paraffin [54,55].

The strength, nature, and relative concentration of acid sites for siliceous were assessed by Landmesser et al. (1998). FTIR spectroscopy was employed to analyze a variety of elements including Ga-, Al-, and Fe-substituted MCM-48, where the target region of the δ_{NH} vibrations of adsorbed ammonia and ν_{OH} vibrations was considered. Note that the internal surface area is highly hydroxylated. In this phase, one can distinguish various kinds of hydroxy groups. For example, 3500 cm^{-1} (associated silanols), 3710 cm^{-1} (geminal silanols), and vibrating at 3740 cm^{-1} (terminal silanols) were observed. The surface is to be intensely hydrophilic; however, silanols are not acidic. Replacement of silicon by Fe, Ga,

and Al, Ga creates Brønsted acid sites. Hence, in the spectra of adsorbed ammonia, a rise to an absorbance at 1450 cm^{-1} is observed [56].

3. Experimental

3.1. Chemicals

Hydrochloric acid (HCl; purity 99%), *n*-heptane (purity 99.33%), $\text{CoN}_2\text{O}_6 \cdot 6\text{H}_2\text{O}$ (99.99%), and tetraethyl orthosilicate (TEOS; purity > 98% (as a source of silica)) were applied as a surfactant. Cetyltrimethylammonium bromide (CTAB; purity > 99%) and Pluronic P123 were supplied by Sigma-Aldrich (Germany). All these chemicals were utilized in their purchased state; no further purification was performed.

3.2. Synthesis of MCM-48

The procedure of formulation explained by [57,58] was performed in the preparation of MCM-48. It was produced using the following steps in a representative synthesis: 10 g of CTAB and 90 g of deionized H_2O were combined. The combination was stirred vigorously at $35\text{ }^\circ\text{C}$ for 40 min. The next step was to add 1 g of NaOH. Following vigorously stirring the combination for 1 h at $35\text{ }^\circ\text{C}$, TEOS was supplied at 11 cm^3 , and the solution was then stirred at that temperature for another 30 min. Finally, the combination was exposed to a heating source in static conditions within an autoclave for 24 h at $150\text{ }^\circ\text{C}$. The prepared MCM-48 product undertakes 1 h of cooling, filtration, distilled water washing, and drying at ambient temperatures. After purification, the synthetic material was calcined at $650\text{ }^\circ\text{C}$ for 6 h through applying a $2\text{ }^\circ\text{C}/\text{min}$ heating ramp rate.

3.3. Loading of Metals onto MCM-48

$\text{Co}(\text{NO}_3)_2 \cdot 6\text{H}_2\text{O}$, a precursor of cobalt, was used to metal-load onto MCM-48 specimens during incipient wetness impregnation (IWI). Metal salt in sufficient quantities (3 wt.% loading) was dissolved in HCl solvent of 0.1 M to generate impregnation solutions, which loaded the metals consisting of a total of 3 wt.% of Co. To maintain metal dispersion at high levels and prevent particle agglomeration as the metal-salt mixture is being vaporized, the whole quantity of solution utilized was equivalent to the overall volume of pores in the support. Following the impregnation process, drying of the catalysts was achieved at room temperature for an overnight period. Following that, the specimen was dried for 24 h in a hot oven at $120\text{ }^\circ\text{C}$, and then the catalyst was subjected to a 4 h calcination process at $500\text{ }^\circ\text{C}$ [57].

3.4. Preparation of Disk MCM-48 Membranes

Prior to installing it inside of the micro-reactor, the catalyst should be firstly pressed into a disk form. The disk shape was made by moulding 0.3 g Co/MCM-48 by loading it into the mould, inserting it inside the pneumatic press mechanism, and pumping it for 5 min at about $5\text{ tonnes}/\text{cm}^2$. The pressed catalyst is installed inside of a micro-reactor constructed of cylindrical Pyrex that is 400 mm in length and 4 mm inside diameter (ID). A suitable amount of glass wool is laid inside the fixed bed reactor to serve as support. This glass wool is introduced into the reactor at a 15 cm-diameter center distance from the upper side of the microreactor. Further glass wool is added into the fixed bed micro-reactor from the top to maintain the catalyst in position.

3.5. Characterization

On a MiniFlex (Rigaku) diffractometer, the small-angle XRD patterns were collected using Cu K radiation ($\lambda = 1.5406\text{ \AA}$) in room conditions. The operating parameters for the X-ray tube were 40 kV and 30 mA, whereas the results were measured with a 2θ step size of 0.01 and a step duration of 10 s, and the results were recorded at $0.5\text{--}8^\circ$ in the 2θ range. Employing a Micrometrics ASAP 2020 pore analyzer, nitrogen adsorption/desorption investigations were conducted at $-196\text{ }^\circ\text{C}$ via N_2 physisorption. Each sample experienced degassing within the sorption analyzer degas port for 3 h at $350\text{ }^\circ\text{C}$ and vacuum ($p < 10^{-5}$

mbar). The BET method was utilized to calculate surface areas of the specimens in the 0.05 to 0.25 range of relative pressures. The Barrett-Joyner-Halenda (BJH) method was applied to determine the distributions of pore sizes, which is based on thermodynamics, from the desorption branch of the isotherm. From the isotherm of the N₂ adsorption branch, the volume of the whole pores was determined as the quantity of liquid nitrogen adsorbed at $P/P_0 = 0.995$. Using BET analysis ($4V/A$), the average mesopore diameters for the specimen were obtained employing nitrogen sorption results. A scanning electron microscope, type JEOL (JSM-5600 LV), was employed to perform scanning electron microscopy (SEM) in analyzing the macropore structure. The combination of EDAX and SEM was used as a technique for analysis that performs an inspection of the elements of the catalyst and identifies its chemical basis. At room temperature, the spectra of infrared of the solid materials (FT-IR) were obtained after being diluted with (8 wt.%) KBr utilizing the transmission mode of the NICOLET 380 FT-IR spectrometer in the 4 cm^{-1} resolution range between 4000 and 400 cm^{-1} .

3.6. Catalytic Test and Isoheptane Measurements

A fixed-bed Pyrex micro-membrane reactor in the configuration of a cylinder with a 400 mm length and a 4 mm ID was loaded with 0.1 g disk catalyst Co/MCM-48 and supported by glass wool inside the reactor. With 50 mL min^{-1} air/H₂, the catalysts were reduced in situ after being calcined in the air at $450\text{ }^\circ\text{C}$ for 4 h. The metal was prevented from sintering and agglomerating across the catalyst in order to achieve optimal performance of the catalyst. The highest temperature heating of $450\text{ }^\circ\text{C}$ and heating rate of $1\text{ }^\circ\text{C min}^{-1}$ are utilized throughout activation. H₂ gas was supplied through the use of a saturator that contained *n*-heptane. The flow rates for H₂ were $20\text{--}45\text{ mL min}^{-1}$ while those for *n*-C₇ were $0.287\text{--}0.686\text{ mL min}^{-1}$. However, the molar concentration of *n*-C₇ in the input stream, as measured through the experiment, was 1.436 mol% and was determined by measuring the feed entire area on the GC-FID during blank tests at flow rates ranging from 20 to 72 mL min^{-1} , utilizing extrapolated *n*-C₇ output factor values. This represented a better fit for the theoretical molar composition determined at $0\text{ }^\circ\text{C}$ using the *n*-C₇ standard vapour pressure and demonstrates that, across the H₂ flow rate range, the saturator is performing extremely close to its optimal value. The catalysts were examined at constant pressures of 100 kPa and a range of temperatures from 250 to $400\text{ }^\circ\text{C}$. The variable volume, constant pressure approach was used to measure the quantity of product mixture gases that permeated across MCM-48 composite membranes, whereas a Varian 3400 GC-FID was used for penetrating gas analysis, which was fitted with either a 50 m Al₂O₃ capillary column of 0.32 mm ID with a 100 kPa feed pressure at 298 K [59].

4. Conclusions

This study employs a dead-end application of an unselective porous catalytic membrane, causing the reactants to flow across the membrane. It serves to create a reaction area with a brief regulated residence duration and strong catalytic activity. Pore diffusion controls the conversion in conventional fixed-bed reactors. Intense contact between the reactants occurs if the catalyst is positioned inside the membrane pores and the reactants flow convectively through the pores.

The MCM-48 catalytic membrane serves as a promising alternative for traditional hydrocracking and hydro-isomerization processes. The introduction of 3 wt.% Co onto a thin MCM-48 layer of protection might enhance the stability of the catalytic membrane against practical scenarios. Other reactions, such as dehydrogenation, can be performed using this membrane reactor technology. Although cobalt commonly shows poor structural, textural, and mechanical characteristics compared to Pt, it is recognized as a great catalyst choice with high activity for isomerization reactions, because of its promising redox features. However, these key properties can be considerably enhanced if this metal is supported on a mesoporous silica like SBA-15, MCM-48, and MCM-41. It was noticed that MCM-48 appears to lack product shape selectivity during isomerization owing to its larger

pores than the products of isomerization and insufficiency of Brønsted acid sites. As a result of the presence of catalysts' Lewis acid sites, the zeolitic catalytic membrane reactor with 3 wt.% Co/MCM-48 demonstrated high selectivity toward cracked products. The findings demonstrate that the majority of produced catalysts can isomerize *n*-C₇ with adequate conversion, selectivity, and stability. The dual pore size distribution of the micro/mesoporous composite catalysts includes both micropores and mesopores. The isomerization of *n*-C₇ is successfully catalyzed by the catalyst composed of 3 wt.% Co/MCM-48. The catalytic activity is reduced as a result of the coke deposition, particularly in the first 1–2 h. The produced catalysts exhibit an appropriate selectivity for both aromatic products and multi-branched isomers. This catalyst has performed well due to its porosity, metal dispersion, acidity, and acid site's nature.

Author Contributions: Conceptualization, N.S.A.; methodology, I.K.S.; software, H.N.H.; validation, H.S.M., J.M.A. and N.M.S.; formal analysis, H.G.S.; investigation, S.Z.; resources, N.S.A. and M.A.A.; data curation, F.T.A.-S.; writing—original draft preparation, T.M.A.; writing—review and editing, K.R.K.; visualization, A.A.-S.; supervision, F.T.A.-S.; project administration, T.M.A.; funding acquisition, H.N.H. All authors have read and agreed to the published version of the manuscript.

Funding: This research was funded by the Dean of Scientific Research at King Khalid University under the grant number RGP2/133/44.

Data Availability Statement: All relevant data and material are presented in the main paper.

Acknowledgments: The authors are grateful to the Department of Chemical Engineering at the University of Technology-Iraq, the Mustansiriyah University/College of Engineering/Materials Engineering Department Baghdad-Iraq, the Department of Chemical and Petroleum Industries Engineering, Al-Mustaqbal University, Babylon, Iraq, and the Department of Civil Engineering, Memorial University of Newfoundland, St. John's, NL A1B 3X5, Canada. The authors extend their appreciation to the Deanship of Scientific Research at King Khalid University of funding this work through large group Research Project under grant number RGP2/133/44.

Conflicts of Interest: The authors declare that they have no competing interest.

References

1. Saracco, G.; Neomagus, H.W.J.P.; Versteeg, G.F.; van Swaaij, W.P.M. High-temperature membrane reactors: Potential and problems. *Chem. Eng. Sci.* **1999**, *54*, 1997–2017. [[CrossRef](#)]
2. Julbe, A.; Farrusseng, D.; Guizard, C. Porous ceramic membranes for catalytic reactors—Overview and new ideas. *J. Membr. Sci.* **2001**, *181*, 3–20. [[CrossRef](#)]
3. Westermann, T.; Melin, T. Flow-through catalytic membrane reactors—Principles and applications. *Chem. Eng. Process. Process Intensif.* **2009**, *48*, 17–28. [[CrossRef](#)]
4. Wang, P.; Liu, H.; Wang, C.; Lv, G.; Wang, D.; Ma, H.; Tian, Z. Direct synthesis of shaped MgAPO-11 molecular sieves and the catalytic performance in *n*-dodecane hydroisomerization. *RSC Adv.* **2021**, *11*, 25364–25374. [[CrossRef](#)] [[PubMed](#)]
5. Jaroszevska, K.; Fedyna, M.; Trawczyński, J. Hydroisomerization of long-chain *n*-alkanes over Pt/AlSBA-15+zeolite bimodal catalysts. *Appl. Catal. B Environ.* **2019**, *255*, 117756. [[CrossRef](#)]
6. Al-Shafei, E.N.; Albahar, M.Z.; Aljishi, M.F.; Akah, A.; Aljishi, A.N.; Alasseel, A. Catalytic conversion of heavy naphtha to reformate over the phosphorus-ZSM-5 catalyst at a lower reforming temperature. *RSC Adv.* **2022**, *12*, 25465–25477. [[CrossRef](#)]
7. Oloye, F.F.; Aliyev, R.; Anderson, J.A. Hydroisomerisation of *n*-heptane over Pt/sulfated zirconia catalyst at atmospheric pressure. *Fuel* **2018**, *222*, 569–573. [[CrossRef](#)]
8. Al-Shathr, A.; Shakor, Z.M.; Majdi, H.S.; AbdulRazak, A.A.; Albayati, T.M. Comparison between Artificial Neural Network and Rigorous Mathematical Model in Simulation of Industrial Heavy Naphtha Reforming Process. *Catalysts* **2021**, *11*, 1034. [[CrossRef](#)]
9. Dai, X.; Cheng, Y.; Si, M.; Wei, Q.; Zhou, Y. Hydroisomerization of *n*-Hexadecane Over Nickel-Modified SAPO-11 Molecular Sieve-Supported NiWS Catalysts: Effects of Modification Methods. *Front. Chem.* **2022**, *10*, 857473. [[CrossRef](#)]
10. Jiang, H.; Li, Z.; Sun, Y.; Jiang, S.; Tian, J. Optimization of the Countercurrent Continuous Reforming Process Based on Equation-Oriented Modeling and the SQP Algorithm. *ACS Omega* **2022**, *7*, 1757–1771. [[CrossRef](#)]
11. Yu, R.; Tan, Y.; Yao, H.; Xu, Y.; Huang, J.; Zhao, B.; Du, Y.; Hua, Z.; Li, J.; Shi, J. Toward *n*-Alkane Hydroisomerization Reactions: High-Performance Pt-Al₂O₃/SAPO-11 Single-Atom Catalysts with Nanoscale Separated Metal-Acid Centers and Ultralow Platinum Content. *ACS Appl. Mater. Interfaces* **2022**, *14*, 44377–44388. [[CrossRef](#)]
12. Chen, Z.; Liu, L.; Shi, F.; Zhou, W.; Yang, Z.; Zhou, A. Hydroisomerization of 1-octene utilizing hierarchical SAPO-11-supported Ni catalysts: Effect of the alkyl chain length of the mesopore. *New J. Chem.* **2022**, *46*, 3901–3908. [[CrossRef](#)]

13. Wang, J.; Liu, C.; Zhu, P.; Liu, H.; Zhang, X. Mercaptosilane-assisted synthesis of highly dispersed and stable Pt nanoparticles on HL zeolites for enhancing hydroisomerization of *n*-hexane. *New J. Chem.* **2022**, *46*, 3482–3492. [[CrossRef](#)]
14. Guo, K.; Ma, A.; Wang, Z.; Li, J.; Wu, B.; Liu, T.; Li, D. Investigation of *n*-heptane hydroisomerization over alkali-acid-treated hierarchical Pt/ZSM-22 zeolites. *New J. Chem.* **2022**, *46*, 16752–16763. [[CrossRef](#)]
15. Naqvi, S.R.; Bibi, A.; Naqvi, M.; Noor, T.; Nizami, A.-S.; Rehan, M.; Ayoub, M. New trends in improving gasoline quality and octane through naphtha isomerization: A short review. *Appl. Petrochem. Res.* **2018**, *8*, 131–139. [[CrossRef](#)]
16. Fedyna, M.; Sliwa, M.; Jaroszewska, K.; Trawczyński, J. Effect of zeolite amount on the properties of Pt/(AISBA-15 + Beta zeolite) micro-mesoporous catalysts for the hydroisomerization of *n*-heptane. *Fuel* **2020**, *280*, 118607. [[CrossRef](#)]
17. Ali, N.S.; Alismael, Z.T.; Majdi, H.S.; Salih, H.G.; Abdulrahman, M.A.; Cata Saady, N.M.; Albayati, T.M. Modification of SBA-15 mesoporous silica as an active heterogeneous catalyst for the hydroisomerization and hydrocracking of *n*-heptane. *Heliyon* **2022**, *8*, e09737. [[CrossRef](#)]
18. Demikhova, N.R.; Rubtsova, M.I.; Kireev, G.A.; Cherednichenko, K.A.; Vinokurov, V.A.; Glotov, A.P. Micro-mesoporous catalysts based on ZSM-5 zeolite synthesized from natural clay nanotubes: Preparation and application in the isomerization of C-8 aromatic fraction. *Chem. Eng. J.* **2023**, *453*, 139581. [[CrossRef](#)]
19. Kapteijn, F.; Wang, X. Zeolite Membranes—The Importance of Support Analysis. *Chem. Ing. Tech.* **2022**, *94*, 23–30. [[CrossRef](#)]
20. Gomez, L.Q.; Shehab, A.K.; Al-Shathir, A.; Ingram, W.; Konstantinova, M.; Cumming, D.; McGregor, J. H₂-free Synthesis of Aromatic, Cyclic and Linear Oxygenates from CO₂. *ChemSusChem* **2020**, *13*, 647–658. [[CrossRef](#)]
21. Gao, X.; Wang, Z.; Chen, T.; Hu, L.; Yang, S.; Kawi, S. State-of-art designs and synthesis of zeolite membranes for CO₂ capture. *Carbon Capture Sci. Technol.* **2022**, *5*, 100073. [[CrossRef](#)]
22. Khadim, A.T.; Albayati, T.M.; Saady, N.M.C. Removal of sulfur compounds from real diesel fuel employing the encapsulated mesoporous material adsorbent Co/MCM-41 in a fixed-bed column. *Microporous Mesoporous Mater.* **2022**, *341*, 112020. [[CrossRef](#)]
23. Ali, N.S.; Harharah, H.N.; Salih, I.K.; Saady, N.M.C.; Zendejboudi, S. Applying MCM-48 mesoporous material, equilibrium, isotherm, and mechanism for the effective adsorption of 4-nitroaniline from wastewater. *Sci. Rep.* **2023**, *13*, 9837. [[CrossRef](#)]
24. Wenten, I.G.; Khoiruddin, K.; Mukti, R.R.; Rahmah, W.; Wang, Z.; Kawi, S. Zeolite membrane reactors: From preparation to application in heterogeneous catalytic reactions. *React. Chem. Eng.* **2021**, *6*, 401–417. [[CrossRef](#)]
25. Alismael, Z.T.; Al-Jadir, T.M.; Albayati, T.M.; Abbas, A.S.; Doyle, A.M. Modification of FAU zeolite as an active heterogeneous catalyst for biodiesel production and theoretical considerations for kinetic modeling. *Adv. Powder Technol.* **2022**, *33*, 103646. [[CrossRef](#)]
26. Dragomirova, R.; Wohlrab, S. Zeolite Membranes in Catalysis—From Separate Units to Particle Coatings. *Catalysts* **2015**, *5*, 2161–2222. [[CrossRef](#)]
27. Ban, Y.; Yang, W. Multidimensional Building Blocks for Molecular Sieve Membranes. *Acc. Chem. Res.* **2022**, *55*, 3162–3177. [[CrossRef](#)]
28. Shi, P.; Li, Z.; Chen, X.; Zeng, L.; Hu, R. Effect of industrial waste molecular sieves on internally cured cement-based materials. *Front. Mater.* **2022**, *9*, 1003556. [[CrossRef](#)]
29. Mittal, N.; Bai, P.; Kelloway, A.; Siepmann, J.I.; Daoutidis, P.; Tsapatsis, M. A mathematical model for zeolite membrane module performance and its use for techno-economic evaluation of improved energy efficiency hybrid membrane-distillation processes for butane isomer separations. *J. Membr. Sci.* **2016**, *520*, 434–449. [[CrossRef](#)]
30. Usman, M. Recent Progress of SAPO-34 Zeolite Membranes for CO₂ Separation: A Review. *Membranes* **2022**, *12*, 507. [[CrossRef](#)]
31. Gora, L.; Jansen, J.C. Hydroisomerization of C₆ with a zeolite membrane reactor. *J. Catal.* **2005**, *230*, 269–281. [[CrossRef](#)]
32. Wang, Y.; Sun, L.; Jiang, T.; Zhang, J.; Zhang, C.; Sun, C.; Deng, Y.; Sun, J.; Wang, S. The investigation of MCM-48-type and MCM-41-type mesoporous silica as oral solid dispersion carriers for water insoluble cilostazol. *Drug Dev. Ind. Pharm.* **2014**, *40*, 819–828. [[CrossRef](#)]
33. Kim, T.-W.; Kleitz, F.; Paul, B.; Ryoo, R. MCM-48-like Large Mesoporous Silicas with Tailored Pore Structure: Facile Synthesis Domain in a Ternary Triblock Copolymer–Butanol–Water System. *J. Am. Chem. Soc.* **2005**, *127*, 7601–7610. [[CrossRef](#)]
34. Olivieri, F.; Castaldo, R.; Cocca, M.; Gentile, G.; Lavorgna, M. Mesoporous silica nanoparticles as carriers of active agents for smart anticorrosive organic coatings: A critical review. *Nanoscale* **2021**, *13*, 9091–9111. [[CrossRef](#)]
35. Yu, Q.; Zhuang, R.; Yi, H.; Gao, W.; Zhang, Y.; Tang, X. Application of MCM-48 with large specific surface area for VOCs elimination: Synthesis and hydrophobic functionalization for highly efficient adsorption. *Environ. Sci. Pollut. Res.* **2022**, *29*, 33595–33608. [[CrossRef](#)]
36. Li, M.; Dong, L.Y.; Li, X.X.; Guo, Z.P.; He, Y.; Lin, Q. Synthesis and Characterization of MCM-48 Molecular Sieves with High Specific Surface Area. *Mater. Sci. Forum* **2021**, *1018*, 147–152. [[CrossRef](#)]
37. Albayati, T.M.; Doyle, A.M. SBA-15 Supported Bimetallic Catalysts for Enhancement Isomers Production During *n*-Heptane Decomposition. *Int. J. Chem. React. Eng.* **2014**, *12*, 345–354. [[CrossRef](#)]
38. Albayati, T.M.; Wilkinson, S.E.; Garforth, A.A. Heterogeneous Alkane Reactions over Nanoporous Catalysts. *Transp. Porous Media* **2014**, *104*, 315–333. [[CrossRef](#)]
39. Al-Nayili, A.; Majdi, H.S.; Albayati, T.M.; Saady, N.M.C. Formic Acid Dehydrogenation Using Noble-Metal Nanoheterogeneous Catalysts: Towards Sustainable Hydrogen-Based Energy. *Catalysts* **2022**, *12*, 324. [[CrossRef](#)]

40. Abukhadra, M.R.; Refay, N.M.; El-Sherbeeney, A.M.; El-Meligy, M.A. Insight into the Loading and Release Properties of MCM-48/Biopolymer Composites as Carriers for 5-Fluorouracil: Equilibrium Modeling and Pharmacokinetic Studies. *ACS Omega* **2020**, *5*, 11745–11755. [[CrossRef](#)]
41. Wang, J.; Wang, G.; Zhang, Z.; Ouyang, G.; Hao, Z. Effects of mesoporous silica particle size and pore structure on the performance of polymer-mesoporous silica mixed matrix membranes. *RSC Adv.* **2021**, *11*, 36577–36586. [[CrossRef](#)]
42. Petrisor, G.; Ficai, D.; Motelica, L.; Trusca, R.D.; Bircă, A.C.; Vasile, B.S.; Voicu, G.; Oprea, O.C.; Semencescu, A.; Ficai, A.; et al. Mesoporous Silica Materials Loaded with Gallic Acid with Antimicrobial Potential. *Nanomaterials* **2022**, *12*, 1648. [[CrossRef](#)]
43. Zhang, K.; Yuan, E.-H.; Xu, L.L.; Xue, Q.-S.; Luo, C.; Albela, B.; Bonneviot, L. Preparation of High-Quality MCM-48 Mesoporous Silica and the Mode of Action of the Template. *Eur. J. Inorg. Chem.* **2012**, *2012*, 4183–4189. [[CrossRef](#)]
44. Petrisor, G.; Motelica, L.; Ficai, D.; Trusca, R.D.; Surdu, V.-A.; Voicu, G.; Oprea, O.C.; Ficai, A.; Andronescu, E. New Mesoporous Silica Materials Loaded with Polyphenols: Caffeic Acid, Ferulic Acid and p-Coumaric Acid as Dietary Supplements for Oral Administration. *Materials* **2022**, *15*, 7982. [[CrossRef](#)]
45. Fathy, M.; Selim, H.; Shahawy, A.E.L. Chitosan/MCM-48 nanocomposite as a potential adsorbent for removing phenol from aqueous solution. *RSC Adv.* **2020**, *10*, 23417–23430. [[CrossRef](#)]
46. Ba-Abbad, M.M.; Kadhum, A.A.H.; Mohamad, A.B.; Takriff, M.S.; Sopian, K. Synthesis and catalytic activity of TiO₂ nanoparticles for photochemical oxidation of concentrated chlorophenols under direct solar radiation. *Int. J. Electrochem. Sci.* **2012**, *7*, 4871–4888. [[CrossRef](#)]
47. Eswaramoorthi, I.; Lingappan, N. Ni–Pt/H-Y Zeolite Catalysts for Hydroisomerization of *n*-Hexane and *n*-Heptane. *Catal. Lett.* **2003**, *87*, 133–142. [[CrossRef](#)]
48. Al-Shathr, A.; Al-Zaidi, B.Y.; Shehab, A.K.; Shakoor, Z.M.; Aal-Kaeb, S.; Gomez, L.Q.; Majdi, H.S.; Al-Shafei, E.N.; AbdulRazak, A.A.; McGregor, J. Experimental and kinetic studies of the advantages of coke accumulation over Beta and Mordenite catalysts according to the pore mouth catalysis hypothesis. *Catal. Commun.* **2023**, *181*, 106718. [[CrossRef](#)]
49. Tan, Y.; Yu, R.; Cheng, J.; Zhao, H.; Du, Y.; Yao, H.; Li, J. Sinter-resistant platinum nanocatalysts immobilized by biochar for alkane hydroisomerization. *Catal. Sci. Technol.* **2021**, *11*, 7740–7750. [[CrossRef](#)]
50. Chica, A.; Corma, A. Hydroisomerization of Pentane, Hexane, and Heptane for Improving the Octane Number of Gasoline. *J. Catal.* **1999**, *187*, 167–176. [[CrossRef](#)]
51. Al-Shathr, A.; Shakor, Z.M.; Al-Zaidi, B.Y.; Majdi, H.S.; AbdulRazak, A.A.; Aal-Kaeb, S.; Shohib, A.A.; McGregor, J. Reaction Kinetics of Cinnamaldehyde Hydrogenation over Pt/SiO₂: Comparison between Bulk and Intraparticle Diffusion Models. *Int. J. Chem. Eng.* **2022**, *2022*, 8303874. [[CrossRef](#)]
52. Wang, Z.; Navarrete, J. Keggin structure and surface acidity of 12-phospho-tungstic acid grafted Zr-MCM-48 mesoporous molecular sieves. *World J. Nano Sci. Eng.* **2012**, *2*, 134. [[CrossRef](#)]
53. Toosi, M.R.; Peyrovi, M.H.; Mondgarian, R. Conversion of *n*-heptane to LPG and aromatics over Mo₂C and W₂C catalysts supported on ZSM-5. *React. Kinet. Catal. Lett.* **2009**, *98*, 133–138. [[CrossRef](#)]
54. Zakumbaeva, G.; Van, T.; Lyashenko, A.; Egizbaeva, R. Catalytic reforming *n*-octane on Pt–Re/Al₂O₃ catalysts promoted by different additives. *Catal. Today* **2001**, *65*, 191–194. [[CrossRef](#)]
55. Van Deelen, T.W.; Harmel, J.M.; Nijhuis, J.J.; Su, H.; Yoshida, H.; Oord, R.; Zečević, J.; Weckhuysen, B.M.; De Jong, K.P. Disk-Shaped Cobalt Nanocrystals as Fischer–Tropsch Synthesis Catalysts Under Industrially Relevant Conditions. *Top. Catal.* **2020**, *63*, 1398–1411. [[CrossRef](#)]
56. Holger, L.; Hendrik, K.; Uwe, K.; Rolf, F. Acidity of substituted mesoporous molecular sieve MCM-48. *J. Chem. Soc. Faraday Trans.* **1998**, *94*, 971–977. [[CrossRef](#)]
57. Doyle, A.M.; Ahmed, E.; Hodnett, B.K. The evolution of phases during the synthesis of the organically modified catalyst support MCM-48. *Catal. Today* **2006**, *116*, 50–55. [[CrossRef](#)]
58. Doyle, A.; Hodnett, B.K. Synthesis of 2-cyanoethyl-modified MCM-48 stable to surfactant removal by solvent extraction: Influence of organic modifier, base and surfactant. *Microporous Mesoporous Mater.* **2003**, *58*, 255–261. [[CrossRef](#)]
59. Hägg, M.B.; Lie, J.A.; Lindbråthen, A. Carbon molecular sieve membranes: A promising alternative for selected industrial applications. *Ann. N. Y. Acad. Sci.* **2003**, *984*, 329–345. [[CrossRef](#)]

Disclaimer/Publisher’s Note: The statements, opinions and data contained in all publications are solely those of the individual author(s) and contributor(s) and not of MDPI and/or the editor(s). MDPI and/or the editor(s) disclaim responsibility for any injury to people or property resulting from any ideas, methods, instructions or products referred to in the content.